Bulletin of the Seismological Society of America, Vol. 93, No. 1, pp. 301–313, February 2003

Strong Ground-Motion Prediction from Stochastic–Dynamic Source Models

by Mariagiovanna Guatteri, P. Martin Mai, Gregory C. Beroza, and John Boatwright

Abstract In the absence of sufficient data in the very near source, predictions of the intensity and variability of ground motions from future large earthquakes depend strongly on our ability to develop realistic models of the earthquake source. In this article we simulate near-fault strong ground motion using dynamic source models. We use a boundary integral method to simulate dynamic rupture of earthquakes by specifying dynamic source parameters (fracture energy and stress drop) as spatial random fields. We choose these quantities such that they are consistent with the statistical properties of slip heterogeneity found in finite-source models of past earthquakes. From these rupture models we compute theoretical strong-motion seismograms up to a frequency of 2 Hz for several realizations of a scenario strike-slip M_w 7.0 earthquake and compare empirical response spectra, spectra obtained from our dynamic models, and spectra determined from corresponding kinematic simulations. We find that spatial and temporal variations in slip, slip rise time, and rupture propagation consistent with dynamic rupture models exert a strong influence on near-source ground motion. Our results lead to a feasible approach to specify the variability in the rupture time distribution in kinematic models through a generalization of Andrews' (1976) result relating rupture speed to apparent fracture energy, stress drop, and crack length to 3D dynamic models. This suggests that a simplified representation of dynamic rupture may be obtained to approximate the effects of dynamic rupture without having to do full dynamic simulations.

Introduction

In this article we consider the prediction of strong ground motion in the near-fault region, by which we mean the area within about 10 km of the rupture, where the directivity effect, the rise time, and the time dependence of slip after rupture lead to ground motion that may be dominated by large pulses of short duration (e.g., Heaton *et al.*, 1995; Sommerville *et al.*, 1997). Parametric scaling relations for strong ground motion, often referred to as "attenuation laws," have been used extensively to predict simple parameters characterizing ground-motion intensity, such as peak ground acceleration or the spectral acceleration (S_a), as a function of earthquake size and distance (e.g., Abrahamson and Silva, 1997). The utility of such attenuation relations in the near-fault region, within about 10 km of the fault, is uncertain for several reasons.

One limitation for the application of such parametric scaling relations so close to a fault arises from the scarcity of strong-motion data at those distances, particularly for large earthquakes. The ground motion in the near-fault region is greatly affected by the complexity in the slip distribution and rupture propagation as all dislocation models of past earthquakes reveal. Therefore, there is reason to believe that there will be important differences in the character of strong ground motion in the near-fault region compared with that farther from the fault. Thus, simply extrapolating ground-motion intensity measures, such as S_a, from more distant locations to the near-fault region might not lead to reliable predictions of ground motion. Moreover, while strong-motion attenuation relations can be modified to take factors such as directivity into account (Sommerville *et al.*, 1997), it is also likely that standard measures of ground-motion intensity may not capture the damage potential of strong ground motion (e.g., Hall and Heaton, 1995).

There is another, more general, reason to take an alternative approach to predicting strong ground motion. The challenges of performance-based engineering will increasingly require that structures be modeled as complex, dynamic, nonlinear multi-degree-of-freedom systems. This task requires the entire time series of strong ground motion as input, rather than any single, simple intensity measure such as the spectral acceleration. Given all of these factors we are forced to use our limited understanding of earthquake behavior to try to predict the nature of ground motion in the near-fault region.

In this article we present a methodology (inspired by the work of Andrews and Boatwright [1998]) that has the potential to make these simulations more accurate. We model the slip distribution in earthquakes as a spatial random field using the method developed by Mai and Beroza (2002). Using spontaneous rupture modeling, we develop a corresponding description of the temporal evolution of slip, that is, the rupture velocity, the rise time, and the slip-velocity function. Although those parameters could be specified independently, there is no guarantee that the resulting model of earthquake rupture would be physically plausible. In our stochastic–dynamic approach we specify the dynamic parameters of the source, that is, the fracture energy and stress drop, as spatial random fields. A spontaneous dynamic rupture once nucleated under these initial conditions provides a self-consistent model of the entire spatiotemporal evolution of slip in an earthquake. Although previous studies have applied dynamic source modeling for near-source strong ground motion prediction (e.g., Inoue and Miyatake, 1998), our procedure provides the capability of generating physically consistent scenario earthquake models. By simulating multiple realizations of a scenario earthquake it should be possible to use seismograms calculated for such dynamic source models to improve predictions of source effects on strong ground motion.

Stochastic–Dynamic Rupture Modeling: Method

Dynamic descriptions of the earthquake source are typically based on models that satisfy elastodynamic equations with a prescribed fracture criterion on a predetermined fault plane (e.g., Andrews, 1976; Mikumo and Miyatake, 1978; Day, 1982a,b; Das and Kostrov, 1987; Harris *et al.*, 1991, Ben-Zion and Rice, 1997). An earthquake is modeled as a dynamically running shear crack that radiates seismic waves. The slipping fault is associated with a drop in shear stress, and the evolution of rupture depends on the initial conditions and the failure criterion. Kinematic descriptions of the earthquake source, on the other hand, specify the slip as a function of space and time without explicit consideration of a physical model for the rupture process. We model spontaneous rupture using a boundary integral method (Boatwright and Quin, 1986; Das and Kostrov, 1987; Quin and Das, 1989) modified to include approximately the effect of the free surface reflection and the effect of vertical heterogeneity (Spudich *et al.*, 1998).

Stress Drop

In all our rupture models we assume a homogeneous distribution of high initial stress τ_o over the fault plane. We constrain the rupture models to be consistent with the slip heterogeneity found in finite-source models of past earthquakes. This is accomplished by imposing the static stress drop distributions derived from slip realizations that are generated using a random-field model of earthquake slip (Mai and Beroza, 2002), in which slip is characterized by a von Karman autocorrelation function with magnitude-dependent correlation length. We generate spatially variable slip distributions using the spectral synthesis method (Pardo-Igùzquiza and Chica-Olmo, 1993), in which the power spectral density of the random field is ascribed, but the phase is random (under the constraint of hermitian symmetry to ensure that the resulting random field is real). The correlation lengths for each slip realization are obtained from the scaling of the correlation length with source parameters. Thus, slip and stress each have a power-law spectrum (with random phase) at wavelengths smaller than the overall source dimensions. The static stress drop distributions are then calculated directly from the slip distributions using the method of Andrews (1980).

Failure Law

We assume that the fault responds to imposed stress following a slip-weakening model in which friction drops from a static level τ_o to a lower dynamic level τ_f over a characteristic distance, D_c, the slip-weakening displacement. The slip-weakening model can be considered to be an approximation of more general fault-constitutive behavior (e.g., Guatteri *et al.*, 2001). Given the initial shear stress, τ_o, the slip-weakening model is described by the stress drop, $\tau_o - \tau_f$, the strength excess, $\tau_p - \tau_o$, and the slip-weakening displacement, D_c, the displacement over which the stress drops from its peak value, τ_p, to its dynamic level, τ_f. The slip-weakening model eliminates the singularity in stress and slip velocity at the crack tip, which is present in elastic-brittle models.

Because in our dynamic modeling we allow only a slip-weakening behavior, we artificially set the very few regions of negative stress drop to act like barriers (Das and Aki, 1977a,b) with zero stress drop and high strength excess (up to 30 MPa). Future work will address this issue by including different constitutive behaviors on the fault that would result in regions with a net sink of energy.

Fracture Energy

Guatteri and Spudich (2000) showed that for a given stress drop distribution the slip-weakening displacement and the strength excess control the rupture velocity and trade-off strongly with one another. The analysis of high-frequency ground-motion data (>2Hz) might help resolve this ambiguity. Andrews (1999) showed that this trade-off does not exist for supershear rupture propagation.

A less ambiguous parameter that can be used to determine the rupture velocity is the fracture energy, G_c, which represents the energy per unit area that is required to extend the crack. Fracture energy is simply the area under the slip-weakening displacement curve above τ_f and, for a given stress drop distribution, may be representative of the resistance of the fault to failure.

In the fully dynamic simulations of this study we describe our dynamic input parameters in terms of stress drop and fracture energy alone. For each model, we initially prescribe the fracture energy distribution obtained from the respective stress drop distribution and spatially homogeneous values of strength excess and slip-weakening distance. Then, by trial and error we perturb the distribution of $\tau_p - \tau_o$ and

D_c on a few selected portions of the fault plane, in order to obtain the fracture energy distribution that results in a sub-shear rupture speed over most part of the fault. The resulting distribution is nonunique. In our modeling the average rupture velocity is about 85% of the shear-wave velocity, which is chosen to be consistent with observations of the average rupture velocity in previous earthquakes. The range of values over which we vary the strength excess and D_c over all models are 2–10 MPa and 0.5–1.1 m, respectively. Our values of fracture energy are also in agreement with fracture energy estimates for past earthquakes (e.g. Aki, 1979; Beroza and Spudich, 1988; Guatteri *et al.*, 2001; J. R. Rice, personal comm.). Ide and Takeo (1997) and Olsen *et al.* (1997) provided estimates of D_c and stress parameters for the 1995 Kobe and Landers earthquakes, respectively, that are also consistent with our fracture energy values.

It is important to note that assuming homogeneous initial stress, variable stress drop, and variable fracture energy is somewhat arbitrary. Other dynamic simulation studies have instead assigned a variable initial stress distribution and uniform frictional and yield stress distributions (Olsen *et al.*, 1997; Peyrat *et al.*, 2001). As barrier models (Das and Aki, 1977a,b; Papageorgiou and Aki, 1983a,b) and asperity models (Lay and Kanamori, 1981) differ in the high-frequency radiation (Madariaga, 1979), so our models may also have a different high-frequency radiation from those having homogeneous resistance and variable initial stress. However, in this study we focus mainly on source effects at relatively low frequencies (≤1 Hz).

Specifying the stress drop distribution, the friction law, and the fracture energy distribution is sufficient to specify the dynamic rupture model, with the only additional parameter being the hypocenter where we force the rupture to initiate by lowering the fault strength. We now illustrate the procedure with some simple examples of dynamic rupture modeling.

Source Models

The realizations of the scenario earthquake we consider are designed to be representative of strike-slip, M_w 7.0 events in California. We assign a fault length $L = 36$ km and a fault width $W = 16$ km determined from recent source-scaling relations for our selected magnitude (Mai and Beroza, 2000). The fault plane is discretized into 960 subfaults (each 0.75×0.75 km). Extrapolating from Andrews and Boatwright (1998) tests based on a finite-difference code, this grid size should result in accurate slip-velocity spectra up to about 1 Hz. We compute ground velocity at the observer locations shown in Figure 1 using the discrete-wavenumber/finite-element method of Olson *et al.* (1984) and Spudich and Archuleta (1987) using a generic rock velocity structure for California (Table 1) derived from Boore and Joyner (1997). We calculate seismograms in the frequency band 0–2.3 Hz and lowpass filter them with a cosine taper between 2 and 2.3 Hz. The ground-velocity time series were sampled at a rate of 0.1 sec.

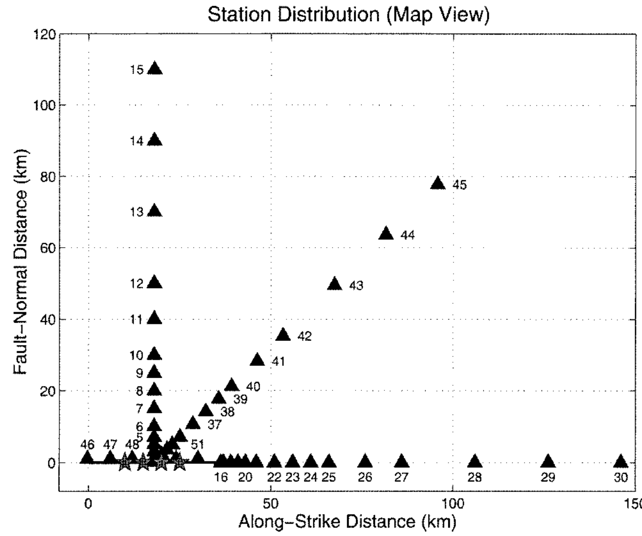

Figure 1. Fault and receiver locations in map view. The fault stretches from 0 to 36 km. Triangles mark receiver locations, and stars mark epicenters for different scenario earthquakes.

Table 1
Velocity Structure

Depth (km)	V_p (km/sec)	V_s (km/sec)	Density (g/cm^3)
0.0	2.40	1.50	2.61
0.5	4.40	2.00	2.66
0.8	4.80	2.40	2.70
1.5	5.30	2.70	2.73
2.2	5.50	2.90	2.74
4.0	5.70	3.30	2.78
8.0	6.06	3.50	2.80
14.0	6.79	3.92	2.80
16.6	7.10	4.10	2.90
27.0	8.00	4.62	3.20
216.0	8.20	4.65	3.20

Although our calculations are accurate only at about 20% at a period of 0.7 sec (Andrews and Boatwright, 1998), in this article we show the respective simulated spectra for the sake of comparison with the corresponding kinematic results. Future work will address accurate high-frequency ground-motion simulations by reducing the fault grid size and by introducing an attenuation factor Q.

We consider three rupture models, A, B, and C, based on three different slip realizations of an earthquake of the same seismic moment, having the same hypocenter at a depth of 11 km and 10 km along-strike. Figure 2 shows the distribution of source parameters for the three models. The top panel shows the spatial distribution of slip on the fault plane (the horizontal axis has been shifted to place the hypocenter at 0 km). The next panel displays the corresponding distribution of static stress drop on the fault plane, followed by the modeled distribution of apparent fracture energy on the fault (third panel). These are the input parameters for dynamic rupture modeling.

Contours of rupture time on the fault plane that arise from the spontaneous rupture calculation, and the local rise time (defined as the time required to accumulate from 10% to 90% of the total slip at a point on the fault), are displayed in panels 4 and 5, respectively. It is important to notice that the variability in the rupture time and rise time distributions is a derived rather than an assumed characteristic of the rupture model. It depends, however, on the assumptions used to obtain the distribution of fracture energy. The result of this exercise is that we now have a complete description of the temporal behavior of the slip during an earthquake that is consistent with the kinematic slip distribution, which is in turn based on the character of slip variation in past earthquakes and represents a plausible approximation to the rupture process.

Same Slip Distribution with Different Hypocenters. As another demonstration, we adopt the slip distribution of model B, but specify three different hypocentral locations at 15, 20, and 25 km along strike and derive a dynamic rupture model as before (shown in Fig. 3). The first two panels (not shown) are the same for all three cases, because they only depend on the static slip (see Fig. 2). The lower three panels are different. The distribution of fracture energy is altered in order to maintain subshear rupture propagation over areas of high slip. In each case, the peak fracture energy is located away from the hypocenter because the rupture will tend to accelerate as it grows due to the increase of the dynamic stress concentration (Andrews, 1976; Day, 1982b). Shifting the hypocenter accounts for the main difference in the rupture time. Figure 4a–c shows the contours of depth-averaged slip-velocity as a function of distance along strike and time for the three new examples, together with reference lines having slopes of 2, 3, and 4 km/sec. These plots show that the average rupture velocity over the fault plane is subshear, as it is locally for main parts of the fault. The width of the contour is indicative of the local slip duration (rise time). Moving the hypocenter position affects the relative time at which different parts of the fault radiate and how waves radiated during slip will interfere with each other. In the following section we also discuss how the location of the hypocenter affects the shape of the slip-velocity function on different parts of the fault.

Source Parameters

Rupture Velocity. To help develop realistic source characterizations, it is important to discuss how rupture velocity is expected to vary over the fault plane for a given slip model. Irregularities in rupture velocity are likely to be the predominant source of high-frequency radiation from propagating faults (Madariaga, 1977; Spudich and Frazer, 1984).

Andrews (1976) obtained an analytical relationship between rupture velocity and fracture energy, stress drop, and crack length valid in simple antiplane strain with uniform stress drop and frictional properties. Even though his relation does not directly apply to 3D heterogenous dynamic simulations, Guatteri and Spudich (2000) have generalized his result to more realistic dynamic models through numerical simulations. In this study we assume that rupture propagation occurs at subshear speed over most parts of the fault, as inferred for the majority of instrumentally recorded earthquakes.

As the crack grows, the rupture tends to accelerate (Andrews, 1976, 1985; Day, 1982a,b) due to the effect of dynamic loading coming from the ruptured area of the fault. Areas of local high stress drop also promote fast rupture propagation. In these areas, relatively large values of fracture energy, corresponding to high fault resistance, are needed to slow down the accelerating rupture growth. The variability in the rupture time distribution is a result both of heterogenous stress drop and fracture energy distributions.

The second set of models (same slip model, varying hypocenter) allows us to study the variability of the rupture velocity. The median values of G_c are comparable (Table 2); however, the locations of area with large values of fracture energy depend on the respective hypocenter locations. As discussed previously, local large values of G_c are necessary as soon as the crack has extended over large distances. From a physical point of view this requirement may seem arbitrary. However, for antiplane rupture, Andrews (1976) showed that energy lost in off-fault microcracking increases with rupture propagation distance. This idea is supported by experimental studies of propagation of single fractures in rocks (Peck *et al.*, 1985) reporting measures of fracture energies typically increasing with crack length until a steady state is reached.

Figure 5a shows the depth-averaged fracture energy for model B (continuous line) and model D3 (dashed line) that represent the two extremes with regard to the effect of hypocenter position on the local rupture velocity. We rewrite equation (23) from Andrews (1976) (notice that in Andrews' equation 23$G = G_c/2$) as follows:

$$1 - v^2/\beta^2 = C(R_c/2)^2, \qquad (1)$$

where R_c is the dimensionless parameter:

$$R_c = \mu G_c/(\Delta\sigma^2 L_h), \qquad (2)$$

where ν is the rupture speed, β is the shear speed, μ is the shear modulus, $\Delta\sigma$ is the stress drop, and L_h is the crack length, which we take to be the distance from the hypocenter. For the case of simple antiplane strain, the constant C is

Table 2
Source Models

	Model A	Model B	Model C	Model D1	Model D2	Model D3
Mean Slip (*m*)	3.6	3.75	3.6	3.9	3.9	3.8
Median G_c (10^6 J/m^2)	4.1	5.1	5	5.6	5.7	5.7

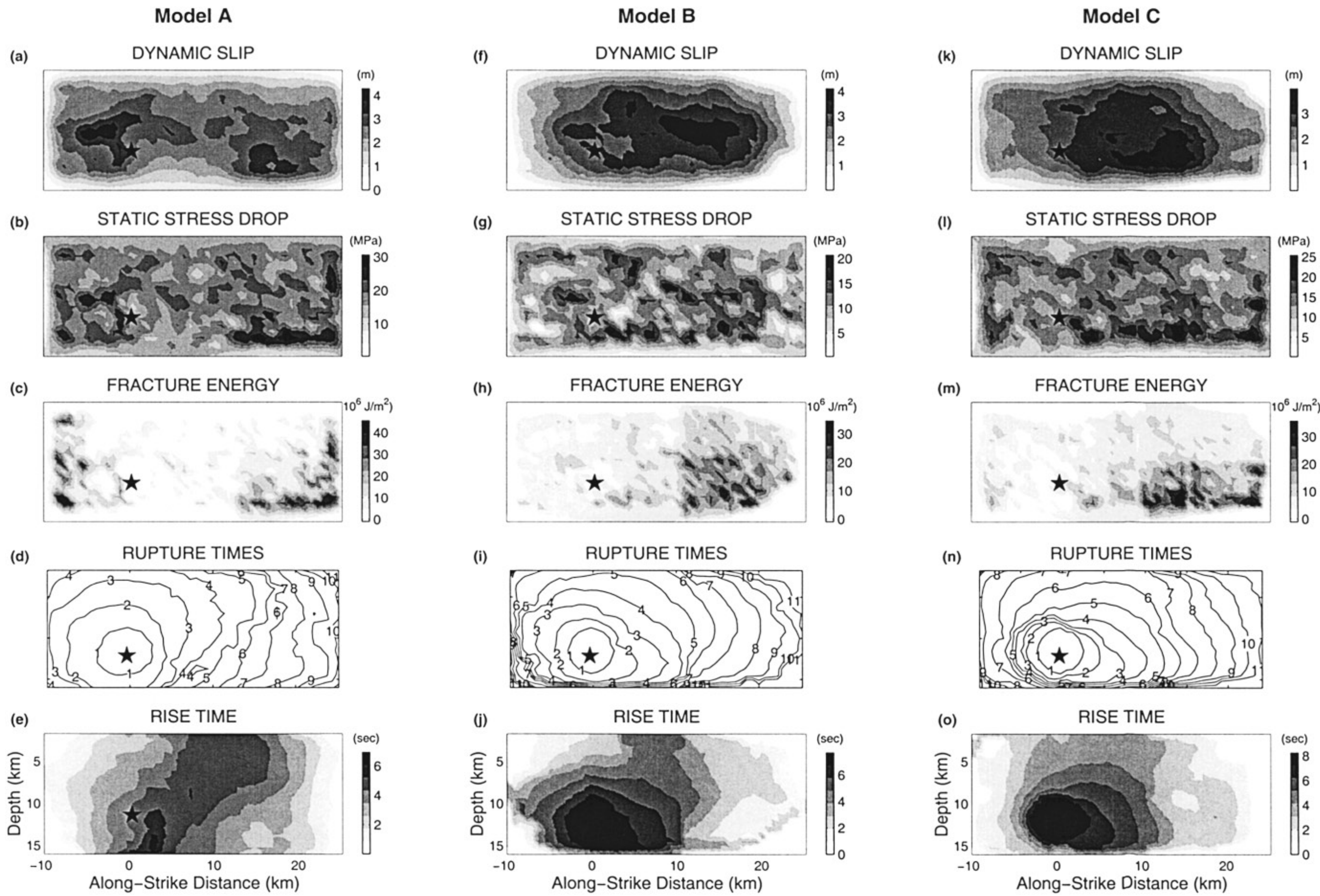

Figure 2. Distribution of kinematic and dynamic source parameters on the fault plane for models A–C (see text). Model A: (a) dynamic slip; (b) static stress drop; (c) fracture energy; (d) rupture times; (e) rise time. Model B: (f) dynamic slip; (g) static stress drop; (h) fracture energy; (i) rupture times; (j) rise times. Model C: (k) dynamic slip; (l) static stress drop; (m) fracture energy; (n) rupture times; (o) rise time.

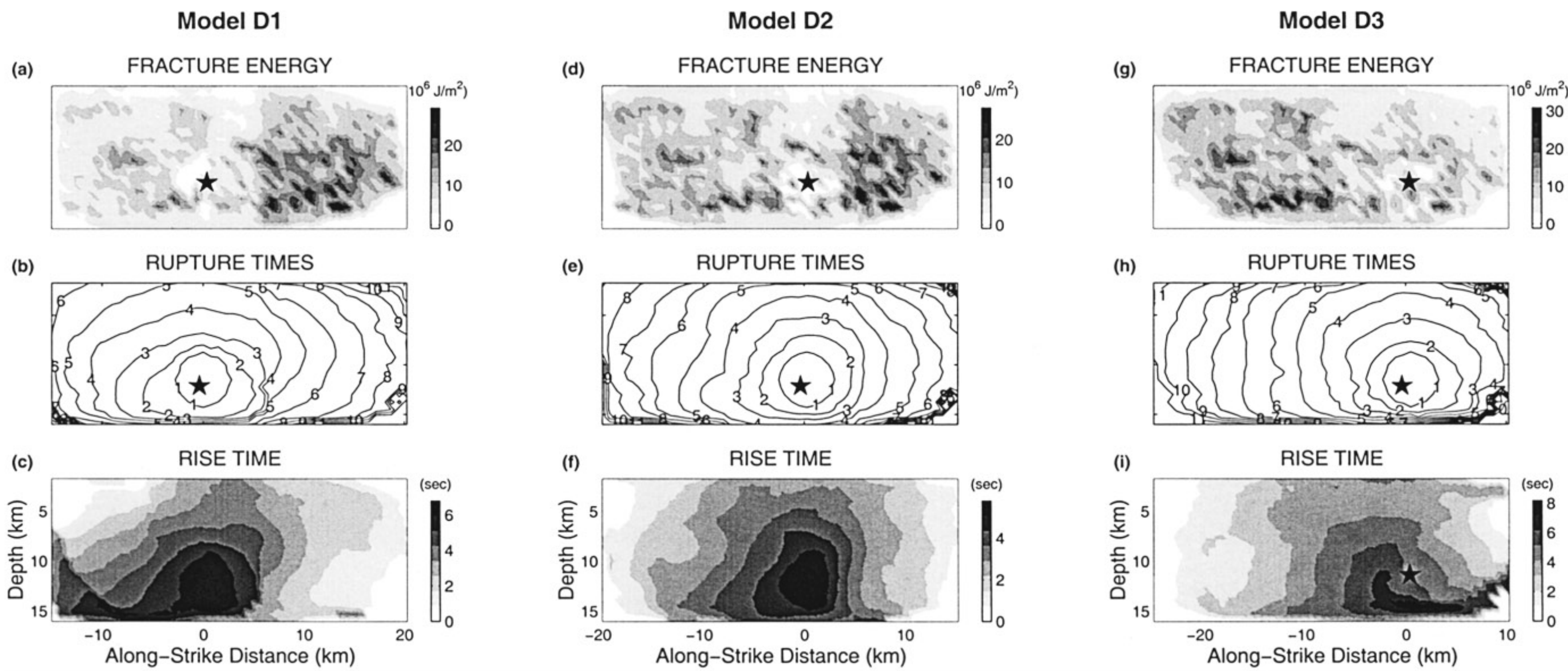

Figure 3. Distribution of parameters on the fault plane for models D1–D3. Slip and stress drop are the same as model B of Figure 2 (see text). Model D1: (a) fracture energy; (b) rupture times; (c) along-strike distance. Model D2: (d) fracture energy; (e) rupture times; (f) rise time. Model D3: (g) fracture energy; (h) rupture times; (i) rise time.

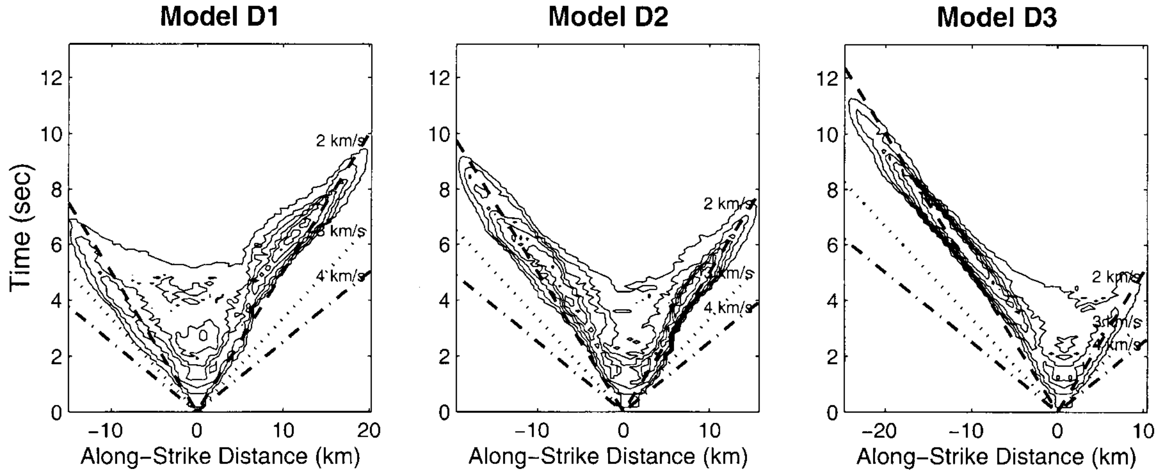

Figure 4. Contours of depth-averaged slip velocity as function of distance along strike and time for models D1, D2, and D3. Three reference rupture velocity lines are shown. The contour lines are at intervals of about 0.3 m/sec.

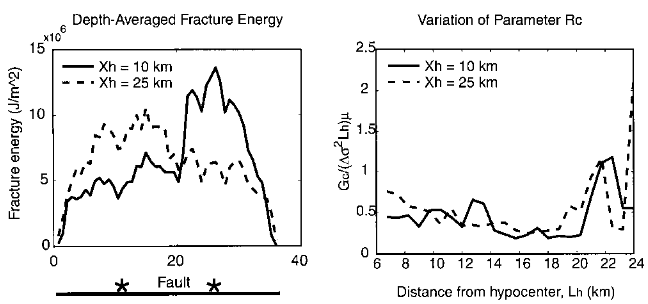

Figure 5. Shown at left is the depth-averaged fracture energy for dynamic rupture models that share the same slip distribution, but with different hypocenters (indicated by stars). X_h is the hypocenter position. Large values of fracture energy are present where it is necessary to slow down rupture propagation. Shown at right is the dimensionless parameter of Andrews (1976) that depends on the fracture energy, G, the stress drop, $\Delta\sigma$, and the distance from the hypocenter (crack length), L_h (note this differs from the along-strike distance). The similarities of this parameter for the two different models suggests that this parameter, which is derived for simple antiplane strain with uniform stress drop, controls the rupture velocity in a 3D, heterogeneous model.

about π^2. Even though model B and model D3 have different hypocenter positions, their rupture speeds are very similar, especially away from the hypocenter ($L_h > 7$ km). In Figure 5b the similarity between the parameter R_c for these two models suggests that Andrews' (1976) relation applies approximately to 3D heterogenous dynamic models. We assume that on average the rupture speed should be approximately 85% of the shear velocity. The median value of R_c for model B is about 0.4, from which we can empirically determine $C \approx 7$, comparable to Andrews' result. This relation may be used to generate realistic rupture time distributions that are consistent with corresponding stress drop distributions in order to design generalized source models for strong ground motion prediction. To test this idea, Mai *et al.* (2001) assumed a homogeneous fracture energy distribution over the fault plane, and based on stress drop and hypocenter location, derived the distribution of the parameter R_c (equation 2), from which they obtained the rupture-velocity distribution (equation 1). Current research addresses the issue of generating nonuniform fracture energy distributions that are physically consistent with a given slip distribution and hypocenter location (Guatteri *et al.*, 2002a,b).

Rise Time and Slip Velocity Function

It is also interesting to compare the slip-velocity functions (SVFs) for the four cases that share the same slip distribution. Figure 6 shows that the slip-velocity functions for the four models (B, D1–D3) are substantially changed when the hypocenter is shifted. Thus, the location of the hypocenter, which has a strong effect on directivity, also has a strong effect on the rise time and the shape of the slip-velocity function (Day, 1982b). It is worth noting that the complex 3D rupture process results in a slip-velocity function that largely resembles the theoretical $t^{-1/2}$-dependence for homogeneous 2D rupture. The spatial variability in the slip-velocity function is not usually considered in kinematic source characterizations for strong-motion prediction; however, it is a reasonable and expected property of a complex rupture model. Large dynamic loading (at points distant from the hypocenter) has the effect of narrowing the SVF, which results in large peak slip velocities. The effect of a local large stress drop is also identifiable and causes similar effects on the slip-velocity function. These examples give some indication of the degree of variability of the SVF over the fault for a relatively complex dynamic rupture model.

In our dynamic simulations, the pattern of variation in the distribution of rise time over the fault (Fig. 2e,j,o and 3c,f,i) is typical for a crack model governed by a slip-

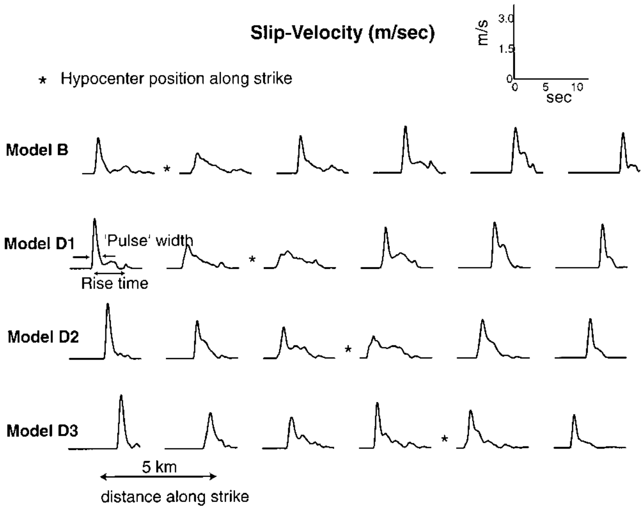

Figure 6. Slip-velocity functions for identical points (each column) on the fault for models B, D1–D3 at a depth of about 9.5 km

weakening law (e.g., Day, 1982b). The rise time is large around the hypocenter and shortens toward the edges of the fault, with values that depend on the total rupture duration. Heterogeneity in the stress parameters adds additional variability in the typical rise time distribution. It is likely that the rise time is being influenced also by scale lengths in the slip and stress drop distribution that vary locally and are substantially smaller than the overall dimensions of the fault. This was shown by Beroza and Mikumo (1996) to be capable of explaining the short rise times inferred for the 1984 Morgan Hill, California, earthquake.

Contrary to simple kinematic parameterizations, because of the more complicated shape of the SVF (Fig. 6), our measured values of rise time might not provide a good quantitative estimate of the time over which the most energetic radiation is released from a given point on the fault. For example, in Figure 6 the SVF of model D1 at 10 km on the left, away from the hypocenter, has a rise time of about 3.5 sec, whereas the most energetic radiation is released in about 1.2 sec, corresponding to the width of the initial slip-velocity pulse. Shortening D_c and increasing the strength excess would have the effect of concentrating the most energetic radiation in a shorter time (Guatteri and Spudich, 2000). However, in this study we mainly concentrate on the intermediate to low frequency range, where these differences are less important, and we chose relatively large values of D_c (0.5–1.1 m) in order to minimize the discretization noise of the dynamic calculation. Later we will discuss how using a shorter D_c affects the simulated response spectra at short periods.

Strong Ground Motion Simulation

The main purpose of this study is to determine what degree of complexity must be included in source models to improve strong ground motion prediction with respect to traditional simple kinematic approaches. Although advanced kinematic procedures have been developed for realistic strong-motion simulations (e.g., Zeng and Anderson, 1994; Saikia and Somerville, 1997; Hisada, 2000, 2001), the assumed source complexity may not be physically plausible. We demonstrate the advantages of a dynamically consistent source characterization over a simple kinematic approach that does not include variability in temporal source parameters by calculating synthetic seismograms for both sets of source models. The choice of the station distribution (Fig. 1) was motivated by the need to simulate strong ground motion in the near-fault region (R $<$ 10 km), where the sparsity of recordings affects the reliability of current parametric scaling relations. At intermediate to large distances, the density of available recordings allows model validation. We compare calculated- and empirical-response spectra (rock sites, 5% damped) using the Abrahamson and Silva (1997) model for strike-slip earthquakes of M_w 7.

Corresponding to each dynamic model, we develop two kinematic source characterizations: the first is based on a hybrid kinematic-dynamic parameterization, and the second is based on a simple kinematic parameterization. For both parameterizations, we assign the original kinematic slip distribution and a boxcar SVF with a rise time of 1 sec over the entire fault plane. In the hybrid parameterization we assign the rupture time distribution derived from the respective dynamic model, whereas in the kinematic model the rupture propagates at a uniform rupture velocity equal to 85% of the local shear speed. Table 3 summarizes the parameterizations and parameter values of the three modeling approaches.

The empirical attenuation relations for crustal earthquakes were derived using a worldwide data set of shallow events (Abrahamson and Silva, 1997). However, only very few recordings from M_w 7 earthquakes constrain these relations at short distances from the fault ($R < 10$ km) where ground motions are potentially the most damaging. Figure 7 shows the comparisons of empirical and simulated spectral acceleration attenuation at several periods for the three different modeling approaches: dynamic, hybrid, and kinematic. For each approach we plot the geometric mean of the two simulated horizontal components of spectral acceleration for all slip models and at all stations excluding those along the fault strike (stations 16–30). These locations are along a nodal plane where only the fault-normal component of motion is different from zero (shown in Fig. 8). We stress that no attempt was made to optimize any of the models. It is interesting to note, however, that near-fault locations show much more variability in the dynamic models than they do in the hybrid or kinematic models. This is attributable to variations in the slip-velocity function arising from rupture dynamics effects and underscores the importance of understanding the slip velocity behavior for predicting strong ground motion in the very near-fault region. In general, the simulations from the kinematic approach underperform those obtained from the dynamic and hybrid modeling. At

Table 3
Summary of Modeling Approaches

	Dynamic	Hybrid	Kinematic
Slip	Dynamic	Kinematic	Kinematic
Rupture Velocity, V	Variable	Variable (from dynamic model)	Uniform, 85% shear wave
Rise Time, T	Variable, mean $\langle T \rangle = 3$ sec	Uniform, $T = 1$ sec	Uniform, $T = 1$ sec
SVF	Variable	Boxcar	Boxcar

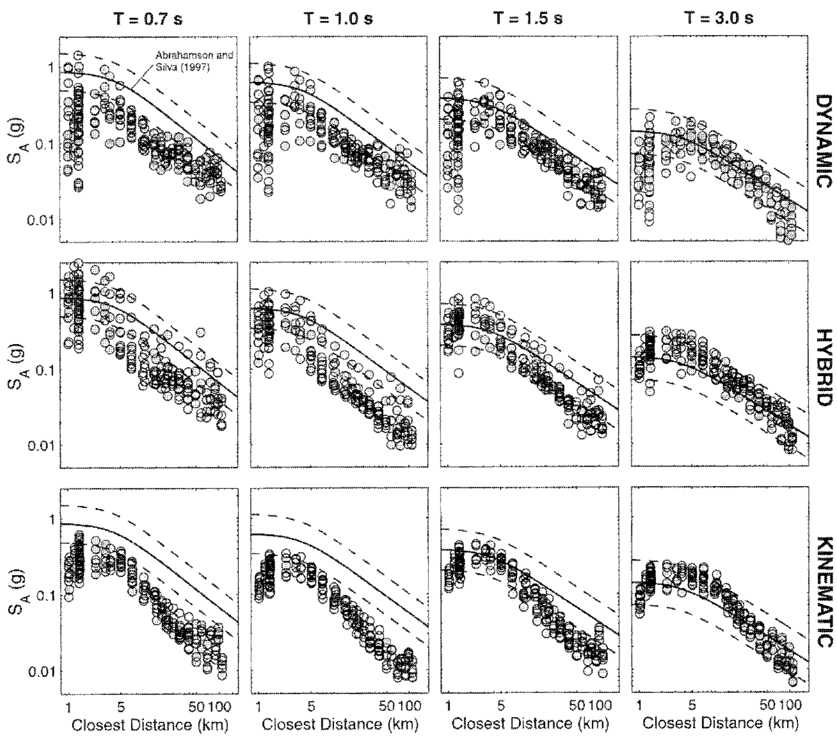

Figure 7. Comparison of simulated (circles) and empirical average horizontal spectral acceleration attenuation (solid line) of Abrahamson and Silva (1997) for a M 7 strike-slip earthquake. Dashed line is the standard deviation of the empirical relation. The simulated values were obtained using the dynamic models: A–C and D1–D3. The hybrid and kinematic simulations were obtained as explained in Table 2. The spectral acceleration for the nodal stations (16–30 in Fig. 1) is not shown here. Hybrid models were obtained by assuming the rupture velocities in the dynamic model, using a constant rise time of 1 sec.

short periods ($T = 0.7$ sec) all the simulated spectral accelerations are depleted in high frequency with respect to the empirical values. This is probably due to the relatively coarse model discretization and the limited frequency band of the Green's functions used in our ground-motion simulation. In general, the hybrid model predicts larger spectral acceleration amplitudes with respect to the other two approaches, especially in the very near-fault region. Although these larger amplitudes correspond to a better agreement with the empirical relation at short periods, they overestimate the long-period values. The dynamic simulations overall follow the slope of the empirical relation better than both the kinematic and hybrid approaches, especially at intermediate distances, where sufficient data exist to provide adequate constraints for the empirical relation.

Directivity Effects

We now discuss directivity effects that cause the ground motions to be strongest on the fault-normal component of motion, particularly in the near-fault region. Strong forward directivity effects occur when the rupture front propagates toward the site. Therefore, among our models, we expect model D3 to result in the smallest forward directivity effects at the nodal stations 16–30.

In Figure 8 we show the fault-normal horizontal component of spectral accelerations calculated at the nodal stations 16–30 for various periods. The values simulated from the three models—D1, D2, and D3—are plotted with different symbols to compare the variations of directivity effects. At all periods, the dynamic simulations capture the variability of directivity effects among the models having different hypocenter positions, showing that model D3 (diamonds) results in the smallest amplitudes, especially in the very near-source region. Surprisingly, the hybrid simulations show these systematic differences only at larger distances ($R > 10$ km), whereas the analysis of the kinematic results does not reveal any substantial difference among the different models. The differences between the dynamic and hybrid simulations are due solely to the different slip-velocity functions, showing that the use of physically consistent slip-

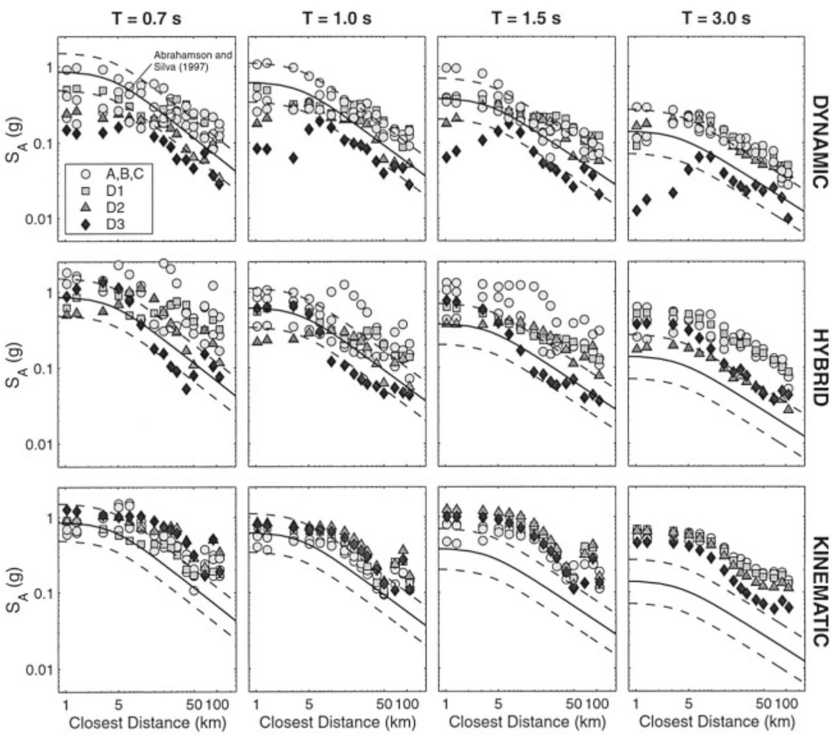

Figure 8. Comparison of simulated fault-normal horizontal component (circles) and empirical attenuation (solid line) of Abrahamson and Silva (1997) for a M 7 strike-slip earthquake. Only the simulated values at the nodal stations 16–30, for which the directivity effects are the largest, are shown.

velocity functions might improve near-source strong ground motion predictions. The comparison with the empirical relation is not straightforward because these fault-normal component amplitudes are not averaged values as are those shown in Figure 7. Nevertheless, we notice that the fall-off of the empirical relation is matched by both the dynamic and hybrid simulated values at intermediate to large distances.

Waveforms and Amplitude Spectra

In Figure 9 we compare ground-velocity seismograms calculated at a near-fault location ($R_{\mathrm{rup}} = 3.2$ km) from the dynamic and kinematic simulations for all five slip models. The higher degree of complexity characteristic of dynamic source models with respect to kinematic models is evident in the resulting waveforms. The kinematic simulations produce very simple waveforms with big similarities between the five different slip models. On the other hand, the dynamic modeling produces complex waveforms with high variability between the five models, presumably providing a more realistic characterization of near-fault ground motion. Notice that the kinematic waveforms have larger peak amplitudes than the dynamic seismograms in which the energy is more spread over the entire signal. Such difference is probably due to the higher degree of coherency in the kinematic source models caused by homogeneity in the rupture velocity, rise time, and slip-velocity function.

We also compare amplitude spectra calculated using the two modeling approaches. Notice that, in general, compared to the kinematic spectra, the dynamic spectra are smoother, having less spectral holes over the high-frequency range (above 1 Hz). Again, this is a result of the higher degree of complexity captured in dynamic simulations.

Discussion

The comparison among the three modeling approaches allows us to infer how specific source characteristics affect the predicted response at various periods, with particular emphasis on the low-frequency range. The systematic large spectral amplitude of kinematic and hybrid simulated responses at long periods reflect the strong coherency of energy release as the rupture propagates along the fault. Among our three classes of models, the kinematic models have the largest degree of coherence due to homogeneous rupture velocity and uniform SVF, whereas the variability in both these parameters in the dynamic models greatly diminishes the coherent energy release during rupture. One peculiarity in the kinematic response spectra at large periods is the lack of decay over distances between 2 and 6 km. We investigated this effect and found that this occurs only for the stations at 45° from the fault line, likely due to enhanced directivity effects caused by source-receiver geometry and homogeneous rupture velocity.

The introduction of spatial and temporal heterogeneity tends to increase peak ground motion amplitudes at short periods. This behavior is manifest in the larger spectral amplitudes simulated from the hybrid and dynamic models with respect to those calculated from the kinematic models at short periods ($T < 2$ sec) in the near-source region. Although the dynamic models are the most complex, the hybrid ap-

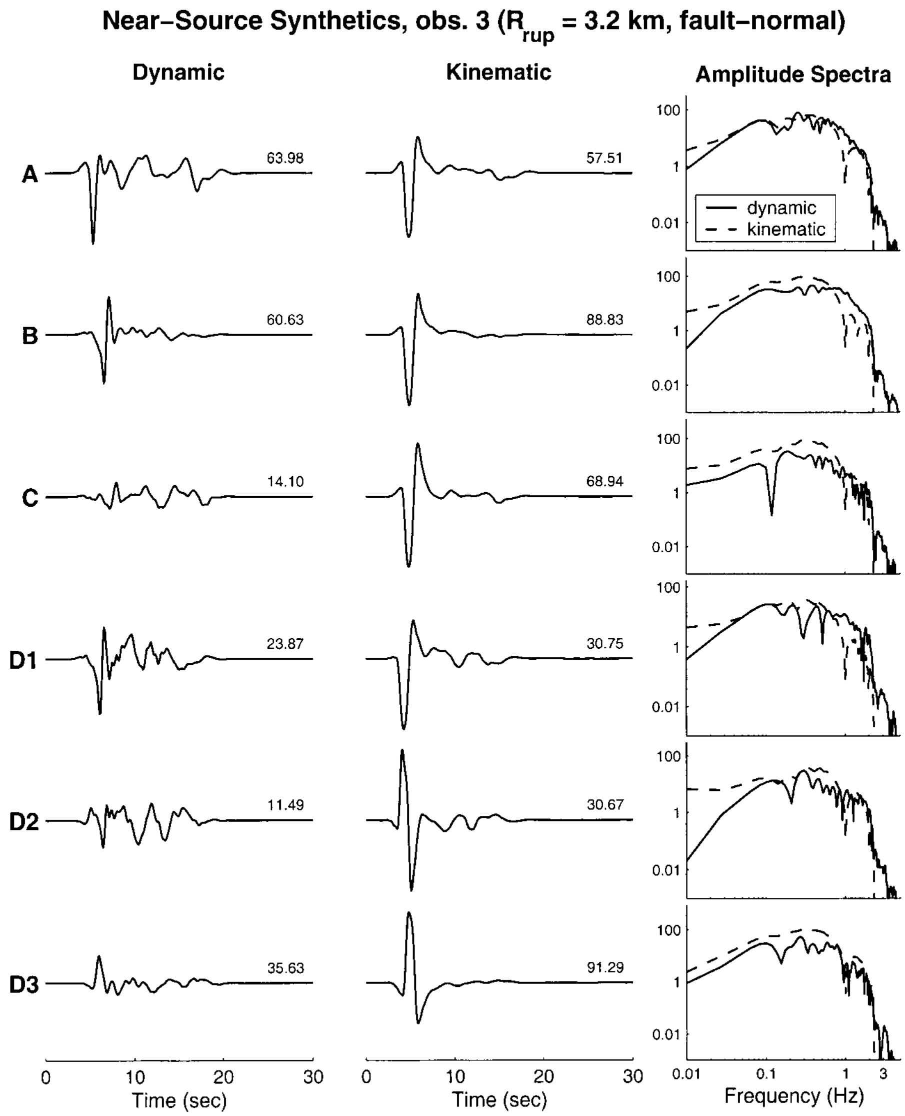

Figure 9. Comparison of simulated ground-velocity at observer 3 (R_{rup} = 3.2 km) from the dynamic models (first column) and kinematic models (second column). The comparison of amplitude spectra is shown in the third column.

proach results in larger high-frequency responses. We interpret this as a consequence of the spectral characteristics of the SVF assumed in the hybrid models (box-car with a rise time of 1 sec). We checked this by calculating ground motions from the hybrid models assuming a rise time of 2 sec and observe a systematic decrease especially in the high-frequency amplitudes. This suggests that the SVF obtained from our dynamic modeling might be too smooth to correctly predict the short-period response.

An interesting feature of the dynamic response spectra is the large range of amplitude variation in the very near-fault region (0.3 and 1 km). Understanding this behavior is important because it occurs in the region where the scarcity of observations requires simulations to complement the available data set. The stations located at these short distances from the source are distributed along the fault, where the ground motion is mainly affected by the local rupture behavior rather than by the whole source. The high degree of heterogeneity and complexity of the dynamic source models, especially in the SVF, accentuates the different characteristics of the seismic radiation affecting each of these near-fault stations for a given source model. The 1999 Chi-Chi, Taiwan, earthquake provides an example of low near-fault observed spectral accelerations with respect to the empirical relations (Boore, 2001). This might be related to the specific local source behavior. Areas with local low stress drop and/or large D_c, which may characterize shallow source regions (e.g., Ide and Takeo, 1997), correspond to areas of local low peak slip-velocity and smooth SVF that, in turn, may result in low amplitude near-fault ground accelerations. On the other hand, kinematic models that do not include such variability in the SVF behavior corresponding to local source properties result in homogeneous ground motions even at different locations along the fault.

The high variability in spectral amplitudes very close to the fault as results from dynamic simulations implies that prediction of ground-motion intensity in the near-source region is subject to a high degree of uncertainty and is highly event specific. Recently, distance-dependent errors have been associated with ground-motion empirical relationships, showing larger prediction errors in the near-fault region (N.A. Abrahamson, personal comm.).

Guatteri and Spudich (2000) showed that a dynamic model having a short slip-weakening distance exhibits more sharply peaked SVFs compared to a corresponding model with a longer D_c. A more strongly peaked SVF results in larger high-frequency ground-motion amplitudes. To test this idea, we have computed response spectra from a dynamic model having the same slip, static stress drop, and fracture energy distributions as in model B, but with a shorter D_c (about a half of the original value). We found that at a period of 0.7 sec, the short D_c model results in systematically larger response spectral amplitudes, particularly at the medium to large distances. An even shorter D_c would result in larger high-frequency amplitudes. Although it is beyond the scope of this study, these results suggest that the analysis of high-frequency spectra may help to constrain rupture dynamics.

Conclusions

This study shows that including variability in all the relevant source parameters, such as slip, rupture velocity, and SVF, has a great effect on the simulated ground motion. The improvement provided by including heterogeneity in the rupture velocity is evident from the comparison between the hybrid and kinematic simulations. An important result of this article is the derivation of a methodology to include variability in the rupture time distribution in kinematic models through a generalization of Andrews' (1976) result relating rupture speed to apparent fracture energy, stress drop, and crack length. Preliminary results of such a pseudodynamic source characterization are very encouraging (Mai *et al.*, 2001; Guatteri *et al.*, 2002). The additional effects of variable SVF in the dynamic models are subtler and probably less evident because of our specific choice of rise time values in the kinematic and hybrid parameterizations. Figure 6 suggests that the assumption that a boxcar describes the time dependence of slip after rupture is inadequate to realistically characterize the fault behavior. A truncated Kostrov function (e.g., Beroza and Spudich, 1988), overlapping triangles (e.g., Wald *et al.*, 1991), or a cosine slip function (Cotton and Campillo, 1995) better describe the fault-particle motion of a complex source. Nakamura and Miyatake (2000) have developed a time-domain parameterization of a dynamically consistent SVF that has great potential for applications to near-field strong ground motion simulations. The empirical relation between slip rise time and magnitude proposed by Somerville *et al.* (1999) determines a median rise time of about 1.5 sec for a M_w 7 earthquake. Our results suggest that this value might be appropriate for the median value of a spatially variable width of the slip-velocity function pulse (Fig. 6).

A weakness of the procedure we have developed is that the fracture energy is specified by trial-and-error modeling. Guatteri *et al.* (2002) addressed this problem through the development of an empirical relationship between fracture energy and known source parameters, such as stress drop and hypocenter location. The results of this study can be applied to develop more physically constrained kinematic source models for deterministic near-fault strong ground motion simulations. A more realistic and robust characterization of the rupture process, in combination with stochastic high-frequency simulations, has the potential to improve the modeling of near-fault ground motions. Physically consistent source characterization of scenario earthquakes should lead to more realistic ground-motion time histories, which in turn should improve our ability to predict the dynamic response of structures to near-fault ground motions.

Acknowledgments

We are very grateful to Joe Andrews, Raul Madariaga, and Paul Spudich for reviewing the manuscript and providing valuable comments and critiques. This research was supported by NSF Grant EAR-0106823.

References

Abrahamson, N. A., and W. J. Silva (1997). Empirical response spectral attenuation relations for shallow crustal earthquakes, *Seism. Res. Lett.* **68,** 94–128.

Andrews, D. J. (1976). Rupture propagation with finite stress in antiplane strain, *J. Geophys. Res.* **81,** 3575–3582.

Andrews, D. J. (1980). Fault impedance and earthquake energy in the Fourier transform domain, *Bull. Seism. Soc. Am.* **70,** 1683–1698.

Andrews, D. J. (1985). Dynamic plane-strain shear rupture with a slip-weakening friction law calculated by a boundary integral method, *Bull. Seism. Soc. Am.* **75,** 1–21.

Andrews, D. J. (1999). Can we infer slip-weakening displacement from seismic observations? *EOS* **80,** no. 66, 755.

Andrews, D. J., and J. Boatwright (1998). Dynamic simulations of spontaneous rupture with heterogeneous stress drop, *Seism. Res. Lett.* **69,** 142.

Ben-Zion, Y., and J. R. Rice (1997). Dynamic simulations of slip on a smooth fault in an elastic solid, *J. Geophys. Res.* **102,** 17,771–17,784.

Beroza, G. C., and T. Mikumo (1996). Short slip duration in dynamic rupture in the presence of heterogeneous fault properties, *J. Geophys. Res.* **101,** 22,449–22,460.

Beroza, G. C., and P. Spudich (1988). Linearized inversion for fault rupture behavior: application to the 1984, Morgan Hill, California, earthquake, *J. Geophys. Res.* **93,** 6275–6296.

Boatwright, J., and H. Quin (1986). The seismic radiation from a 3-D dynamic model of a complex rupture process, Part 1. Confined rupture, in *Earthquake Source Mechanics*, S. Das, J. Boatwright, and C. Scholz (Editors), American Geophysical Union, Washington, D.C.

Boore, D. M. (2001). Comparison of ground motions from the 1999 Chi-Chi earthquake with empirical predictions largely based on data from California, *Bull. Seism. Soc. Am.* **91,** 1212–1217.

Boore, D. M., and W. B. Joyner (1997). Site amplifications for generic rock sites, *Bull. Seism. Soc. Am.* **87,** 327–341.

Cotton, F., and M. Campillo (1995). Frequency domain inversion of strong motions: application to the 1992 Landers earthquake, *J. Geophys. Res.* **100,** 3961–3975.

Das S., and K. Aki (1977a). A numerical study of two-dimensional spontaneous rupture propagation, *Geophys. J. R. Astr. Soc.* **50,** 63–668.

Das, S., and K. Aki (1977b). Fault plane with barriers: a versatile earthquake model, *J. Geophys. Res.* **82,** 5658–5669.

Das, S., and B. V. Kostrov (1987). On the numerical boundary integral equation method for three-dimensional dynamic shear crack problems, *J. Appl. Mech.* **54,** 99–104.

Day, S. M. (1982a). Three-dimensional finite difference simulation of fault dynamics: rectangular faults with fixed rupture velocity, *Bull. Seism. Soc. Am.* **72,** 705–727.

Day, S. M. (1982b). Three-dimensional simulation of spontaneous rupture: the effect of nonuniform prestress, *Bull. Seism. Soc. Am.* **72,** 1881–1902.

Guatteri, M., and P. Spudich (2000). What can strong motion data tell us about slip-weakening fault-friction laws? *Bull. Seism. Soc. Am.* **90,** 98–116.

Guatteri, M., P. M. Mai, and G. C. Beroza (2002). Dynamic and pseudo-dynamic source characterization for strong ground motion prediction, *EOS* **83,** 1058.

Guatteri, M., P. Spudich, and G. C. Beroza (2001). Inferring rate and state friction parameters from a rupture model of the 1995 Hyogo-ken Nanbu (Kobe) earthquake, *J. Geophys. Res.* **106,** 26,511–26,522.

Hall, J. F., and T. H. Heaton (1995). Near-source ground motion and its effects on flexible buildings, *Earthquake Spectra* **11,** 569–605.

Harris, R. A., R. J. Archuleta, and S. M. Day (1991). Fault steps and the dynamic rupture process: 2-D numerical simulations of a spontaneously propagating shear fracture, *Geophys. Res. Lett.* **18,** 893–896.

Heaton, T. H., J. F. Hall, D. J. Wald, and M. J. Halling (1995). Response of high-rise and base-isolated buildings to a hypothetical M_w 7.0 blind thrust earthquake, *Science* **267,** 206–211.

Hisada, Y. (2000). A theoretical omega-square model considering the spatial variation in slip and rupture velocity, *Bull. Seism. Soc. Am.* **90,** 387–400.

Hisada, Y. (2001). A theoretical omega-square model considering the spatial variation in slip and rupture velocity. II. Case for a two-dimensional source model, *Bull. Seism. Soc. Am.* **91,** 651–666.

Ide, S., and M. Takeo (1997). Determination of constitutive relations of fault slip based on seismic wave analysis, *J. Geophys. Res.* **102,** 27,379–27,391.

Inoue, T., and T. Miyatake (1998). 3D simulation of near-field strong ground motion based on dynamic modeling, *Bull. Seism. Soc. Am.* **88,** 1445–1456.

Lay, T., and H. Kanamori (1981). An asperity model of great earthquake sequences, in *Earthquake Prediction, An International Review*, D. Simpson and P. Richards (Editors), American Geophysical Union, Washington, D.C., Maurice Ewing Series, Vol. 4 579–592.

Madariaga, R. (1977). High-frequency radiation from crack (stress-drop) models of earthquake faulting, *Geophys. J.* **51,** 625–651.

Madariaga, R. (1979). On the relation between seismic moment and stress drop in the presence of stress and strength heterogeneity, *J. Geophys. Res.* **84,** 2243–2250.

Mai, P. M., and G. C. Beroza (2000). Source scaling properties from finite-fault-rupture models, *Bull. Seism. Soc. Am.* **90,** 604–615.

Mai, P. M., and G. C. Beroza (2002). A spatial random field model to characterize complexity in earthquake slip, *J. Geophys. Res.* **107,** no 81, 2308.

Mai, P. M., M. Guatteri, and G. C. Beroza (2001). A stochastic-dynamic earthquake source model for strong-motion prediction: earthquake scenarios on the Hayward-Rodgers-Creek fault system, *EOS* **82,** 869.

Mikumo, T., and T. Miyatake (1978). Dynamical rupture process on a three-dimensional fault with non-uniform friction and near-field seismic waves, *Geophys. J. R. Astr. Soc.* **54,** 417–438.

Nakamura, H., and T. Miyatake (2000). An approximate expression of slip velocity time functions for simulation of near-field strong ground motion, *Zishin (J. Seism. Soc. Jpn.)* **53,** 1–9 (in Japanese).

Olsen, K. B., R. Madariaga, and R. J. Archuleta (1997). Three-dimensional dynamic simulation of the 1992 Landers earthquake, *Science* **278,** 834–837.

Olson, A. H., J. A. Orcutt, and G. A. Frazier (1984). The discrete wave-number finite element method of synthetic seismograms, *Geophys. J. R. Astr. Soc.* **77,** 421–460.

Papageourgiou, A. S., and K. Aki (1983a). A specific barrier model for the quantitative description of inhomogeneous faulting and the prediction of strong ground motion, part I: Description of the model, *Bull. Seism. Soc. Am.* **73,** 693–722.

Papageourgiou, A. S., and K. Aki (1983b). A specific barrier model for the quantitative description of inhomogeneous faulting and the prediction of strong ground motion, part II: Applications of the model, *Bull. Seism. Soc. Am.* **73,** 953–978.

Pardo-Igùzquiza, E., and M. Chica-Olmo (1993). The Fourier integral method: an efficient spectral method for simulation of random fields, *Mathemat. Geol.* **25,** 177–217.

Peck, L., R. C. Nolen-Hoeksema, C. C. Barton, and R. B. Gordon (1985). Measurement of the resistance of imperfectly elastic rock to the propagation of tensile cracks, *J. Geophys. Res.* **90,** 7827–7836.

Peyrat, S., K. B. Olsen, and R. Madariaga (2001). Dynamic modeling of the 1992 Landers earthquake, *J. Geophys. Res.* **106,** 26,467–26,482.

Quin, H. R., and S. Das (1989). A hybrid boundary integral equation method for the computation of source time functions for 3D rupture propagation, *Geophys. J. R. Astr. Soc.* **96,** 163–177.

Saikia, C. K., and P. G. Somerville (1997). Simulated hard-rock motions in Saint Louis, Missouri, from large New Madrid earthquakes ($M_w \geq 6.5$), *Bull. Seism. Soc. Am.* **87,** 123–139.

Somerville, P. G., K. Irikura, R. Graves, S. Sawada, D. Wald, N. Abrahamson, Y. Iwasaki, T. Kagawa, N. Smith, and A. Kowada (1999). Characterizing crustal earthquake slip models for the prediction of strong ground motion, *Seism. Res. Lett.* **70,** 59–80.

Somerville, P. G., N. F. Smith, R. W. Graves, and N. A. Abrahamson (1997). Modification of empirical strong ground motion attenuation relations to include the amplitude and duration effects of rupture directivity, *Seism. Res. Lett.* **68,** 199–222.

Spudich, P., and R. J. Archuleta (1987). Techniques for earthquake ground-motion calculation with applications to source parameterization of finite faults, in *Seismic Strong Motion Synthetics*, B. A. Bolt (Editor), Academic Press, New York.

Spudich, P., and N. Frazer (1984). Use of ray theory to calculate high-frequency radiation from earthquake sources having spatially variable rupture velocity and stress drop, *Bull. Seism. Soc. Am.* **74,** 2061–2082.

Spudich, P., M. Guatteri, K. Otsuki, and J. Minagawa (1998). Use of fault striations and dislocation models to infer tectonic shear stress during the 1995 Hyogo-ken Nanbu (Kobe) earthquake, *Bull. Seism. Soc. Am.* **88,** 413–427.

Wald, D. J., T. H. Heaton, and K. W. Hudnut (1996). The slip history of the 1994 Northridge, California earthquake determined from strong motion, teleseismic, GPS, and leveling data, *Bull. Seism. Soc. Am.* **86,** 49–70.

Zeng, Y., J. G. Anderson, and G. Yu (1994). A composite source model for computing realistic synthetic strong ground motions, *Geophys. Res. Lett.* **21,** 725–728.

Department of Geophysics
Stanford University
397 Panama Mall
Stanford, California 94305-2215
patti@pangea.stanford.edu
(M.G., P.M.M., G.C.B.)

U.S. Geological Survey
345 Middlefield Rd. MS977
Menlo Park, California 94025
(J.B.)

Manuscript received 11 January 2002.